Bulletin of the Czech Geological Survey, Vol. 77, No. 2, 135–145, 2002

Trace elements and growth patterns in quartz: a fingerprint of the evolution of the subvolcanic Podlesí Granite System (Krušné hory Mts., Czech Republic)

AXEL MÜLLER[1] – ANDREAS KRONZ[2] – KAREL BREITER[3]

[1]Natural History Museum, Dept. Mineralogy, Cromwell Road, London SW7 5BD, United Kingdom; e-mail: A.Mueller@nhm.ac.uk
[2]Geowissenschaftliches Zentrum Göttingen, Goldschmidtstr. 1, D-37077 Göttingen, Germany
[3]Czech Geological Survey, Geologická 6, 152 00 Praha 5, Czech Republic

Abstract. The Podlesí Granite System (PGS) in the Western Krušné hory Mts., Czech Republic, represents a suite of late-Variscan, highly fractionated rare-metal granites. Based on textural studies and cathodoluminescence five igneous quartz populations can be distinguished in the stock granite and the more evolved dyke granite hosting line rocks (layered granites). Trace element profiling by electron probe micro-analysis (EPMA) gives evidence for three main crystallisation stages: (1) the zoned quartz phenocrysts representing the early stage of magma evolution in the middle crust, (2) the stockscheider quartz and groundmass quartz of the stock granite reflecting the subvolcanic solidification conditions of the stock granite, and (3) the zoned snowball quartz and comb quartz of the dyke granite crystallised from a highly evolved, residual melt. Ti and Al in quartz show a general temporal trend reflecting the evolution of the magma: decrease of Ti and increase of Al. The increase of lithophile elements (Li, Na, Al, P, K) and of the water content in the magma, the decrease of Ti, crystallisation temperature and pressure are assumed to be predominantly responsible for the trend. High Al in quartz (>500 ppm) may also result from high crystal growth rate. The textural varieties of the PGS in general are not a product of metasomatic overprinting, but a product of crystallisation of different fractionated melts.

Key words: granite, Krušné hory Mts., quartz population, magma evolution, residual melt, trace elements, zoned quartz

Introduction

Quartz crystals in igneous rocks record and archive stages of magma evolution which can be decoded by means of understanding the trace element signature, intragranular growth pattern, crystal habit and crystal size distribution.

This study concerns the igneous quartz populations of the Podlesí Granite System (PGS), which is located in the Western Krušné hory Mts., Czech Republic. The PGS represents highly fractionated rare-metal granite and provides one of the most impressive exposures of rock assemblages including line rocks (layered granites) developed at the interface between late-magmatic and hydrothermal processes.

Line rocks found at the roof of shallow felsic intrusions are often associated with rare-metal mineralisation (e.g. Shannon et al. 1982, Kirkham and Sinclair 1988, Lowenstern and Sinclair 1996, Balashov et al. 2000, Reyf et al. 2000, Breiter 2002). The rock type is characterised by repeated bands of coarse-grained, euhedral quartz and/or K-feldspar separated by bands of fine-grained granite. Shannon et al. (1982) used the metallurgical term "unidirectional solidification textures" (UST) to describe this layered texture that forms by growth inward from, and perpendicular to, the outer edge of the intrusion.

A central question regarding the genesis of such evolved subvolcanic systems is whether they obtained their chemical and textural signature during the magmatic stage or during subsolidus modification of an igneous or foreign fluid phase or a mixture of both. In recent years the understanding of the complex granite system of Podlesí became progressively more appreciated as studies of whole rock, major and accessory minerals, rock and mineral physics, and melt inclusions accumulated a great body of new data (Breiter et al. 1997, Chlupáčová and Breiter 1998, Táborská and Breiter 1998, Breiter 2001).

To further contribute to this knowledge we studied trace elements in quartz by electron probe micro-analysis (EPMA) and intra-granular growth patterns by cathodoluminescence (CL) to understand the textural and compositional variation of the system, and to distinguish between magmatic and metasomatic processes. Cathodoluminescence (CL) is a sensitive method for revealing growth zoning and different populations of igneous quartz (e.g. Schneider 1993, Watt et al. 1997, D'Lemos et al. 1997, Müller et al. 2000). Recently, EPMA proves to be an effective in situ micro-beam technique to obtain analysis of Ti and Al in zoned quartz, because of the high spatial resolution down to 5 μm and the capability of combining the position of spot analyses with CL imaging (Müller and Seltmann 1999, Müller et al. 2000, Van den Kerkhof et al. 2001, Müller et al. 2002).

Geology, petrography and whole rock chemistry

The Podlesí Granite System (PGS) is a tongue-shaped body in the late-Variscan Eibenstock-Nejdek pluton (Western Krušné hory Mts.; Fig. 1). The top of the granite cupola outcrops over an area of about 0.1 km^2. The internal structure of the copula has been studied through drilling by the Czech Geological Survey (Lhotský et al. 1988, Breiter 2001) and is well exposed in an abandoned quarry.

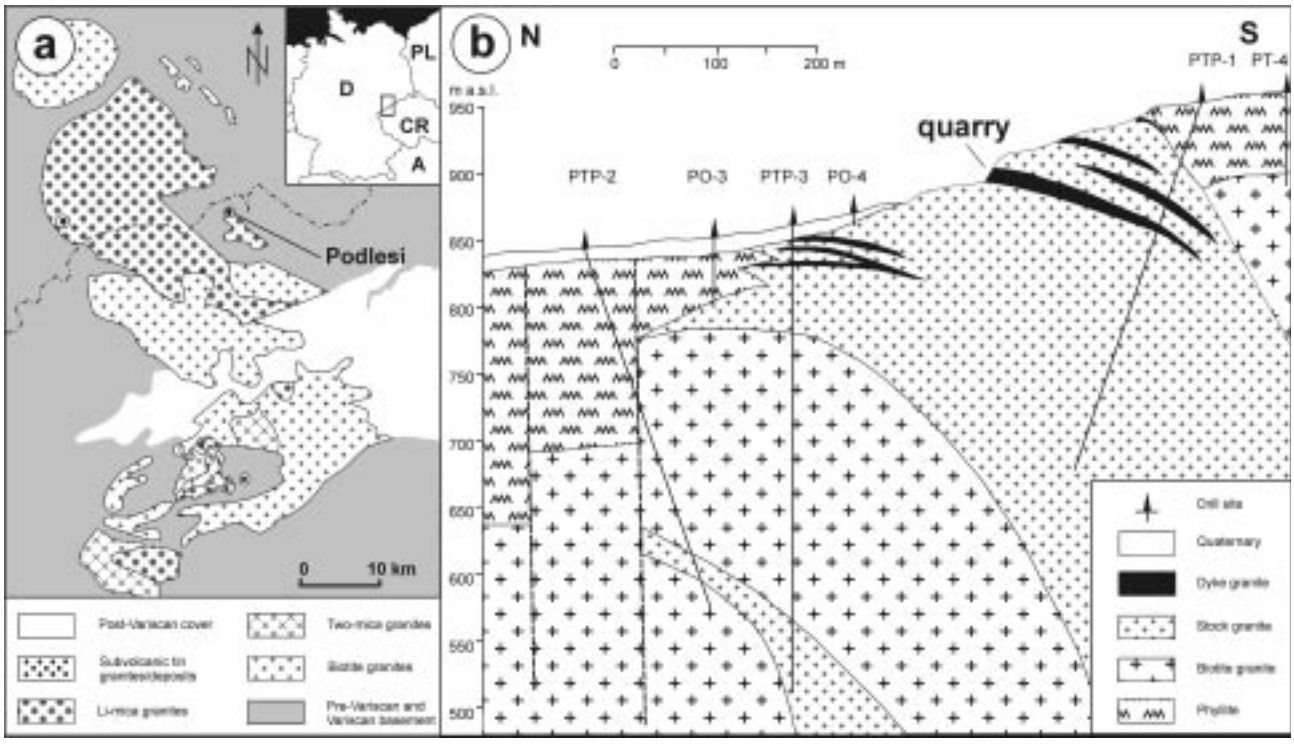

Fig. 1. a – Geological map of the Western Krušné hory/Erzgebirge with the distribution of late-Variscan granites and the location of the Podlesí Granite System (PGS); b – Geological cross-section of the PGS from Breiter (2001).

The PGS intruded Ordovician phyllites and biotite granite ~320 Ma ago (Förster 2001). General petrologic and geochemical characteristics of the PGS are reported by Breiter et al. (1997) and Breiter (2001).

The PGS is mainly formed of albite-protolithionite-topaz granite, named traditionally as *stock granite* (Lhotský et al. 1988, Breiter et al. 1997). Protolithionites (in sense of Weiss et al. 1993) are Li-rich micas but poorer in Li and richer in Fe than zinnwaldite. The uppermost 30–40 m of the stock granite is fine-grained and porphyritic, whereas the main part of the stock consists of medium-grained granite (Fig. 2a). The sharp contact of the granite cupola with the phyllites is bordered by a marginal, 50 cm thick pegmatite (stockscheider; Fig. 2b). The stock granite is peraluminous (A/CNK 1.15–1.25), enriched in incompatible elements such as Li, Rb, Cs, Sn, Nb, W and in phosphorus and fluorine (Breiter et al. 1997, Breiter 2001, Table 1).

Within the depth of 40–100 m the stock granite is intercalated with sub-horizontal layers of albite-zinnwaldite-topaz granite (Fig. 2c). This leucocratic, fine-grained *dyke granite* contains K-feldspar, small isometric quartz crystals, and inclusion-rich topaz that are embedded in fine-grained albite tablets. Borders of larger K-feldspars are often replaced by quartz, albite, and topaz. The dyke granite is more evolved than the stock granite and is relatively enriched in Al (A/CNK 1.2–1.4), P, F, Na, Rb, Li, Nb, and Ta.

Unidirectional solidification textures (UST) are developed in the upper 50 cm of the major layer of dyke granite, which has a thickness of about 6 m. The UST consist of alternating laminae of dyke granite with inhomogeneous chemical composition (Breiter 2001) and of oriented fan-like zinnwaldite with comb quartz (in sense of Shannon et al. 1982; Fig. 2d). Locally, ongrowths of oriented K-feldspar megacrysts (6 cm) on the zinnwaldite-comb quartz layers are developed forming pegmatite-like bands. Directional growth of pegmatitic comb quartz, zinnwaldite, and K-feldspar indicates downward solidification.

The samples investigated were mostly collected in the quarry of Podlesí (Fig. 1b). The stockscheider was sampled at the contact with the host rock, 150 m SE from the quarry.

Methods

Trace element abundances of Al, Ti, K, and Fe in quartz were performed with a JEOL 8900 RL electron microprobe at the GZG Göttingen equipped with 5 WD detectors and with a CL detector using an extended wavelength range from 200 to 900 nm.

SEM-CL images were collected from the JEOL system using slow beam scan rates of 20 s at processing resolution of 1024 × 860 pixels and 256 grey levels. The electron beam voltage and current was 30 kV and 200 nA, respectively. CL imaging prior to and after EPMA analysis allowed the location of the sampling spots in relation to the CL structures.

The following standards were used for the analysis:

Table 1. Major and trace element data of representative whole rock samples from the PGS (from Breiter 2001).

Rock	stockgranite	pegmatite (stockscheider)	dyke granite	pegmatite-like band of the UST
location	quarry Podlesí	150 m SE of quarry Podlesí	quarry Podlesí	quarry Podlesí
Sample No.	709	3361	3413	3417
major elements (wt%)				
SiO_2	73.57	74.78	72.52	66.54
TiO_2	0.04	0.05	0.01	0.02
Al_2O_3	14.93	13.80	15.98	17.79
Fe_2O_3	0.15	0.41	0.01	0.15
FeO	0.66	0.46	0.55	0.94
MnO	0.019	0.03	0.04	0.05
MgO	0.05	0.05	0.04	0.02
CaO	0.27	0.43	0.17	0.39
Li_2O	0.24	0.03	0.29	0.44
Na_2O	3.81	3.60	4.89	2.90
K_2O	3.97	4.23	3.51	6.42
Rb_2O	0.18	0.07	0.22	0.30
P_2O_5	0.43	0.40	0.52	0.80
CO_2	0.01	0.03	0.01	0.01
F	1.35	0.50	1.33	1.72
H_2O^+	1.12	0.88	0.90	1.55
H_2O^-	0.10	0.23	0.14	0.12
F=O	–0.57	–0.21	-0.56	-0.72
total	100.54	99.86	100.83	99.80
trace elements (ppm)				
Ba	n.a.	23	9	12
Cs	103	56	159	198
Hf	2	2	2	2
Nb	47	58	54	79
Sn	62	20	35	31
Sr	47	12	53	87
Ta	19	19	20	54
Th	6	8	6	12
U	11	43	13	29
W	21	24	23	55
Zr	28	31	25	21

n.a. – not analysed

synthetic Al_2O_3 (52.92 wt% Al), orthoclase, Lucerne, Switzerland (12.18 wt% K), synthetic TiO_2 (59.95 wt% Ti), and haematite, Rio Marina, Elba (69.94 wt% Fe). Raw analyses were converted into concentrations, after making appropriate matrix corrections using the phi-rho-z method of Armstrong (1991). For high precision and sensitivity, an accelerating voltage of 20 kV, a high beam current of 80 nA, a beam diameter of 5 µm, and counting times of 15 sec for Si, and of 300 sec for Ti, K, and Fe were chosen. Counting times for the lower background and for the upper background were 150 sec for these elements. Due to the strong drift of the background signal in the low energy range near the Al Kα-line during long counting times the total acquisition of Al x-ray counts was separated in 5 individual steps with a 60 sec peak, 30 sec lower background and 30 sec upper background. This procedure minimises the systematic error coming from a drift of the analysed rays due to beam induced damage of the quartz. The higher energies of the K Kα, Ti Kα and Fe Kα lines are not showing any significant shift of the background signals during the counting time.

Limits of detection (LOD) were 15 ppm for Ti, 11 ppm for K, 15 ppm for Fe, 51 ppm for Na, and 10 ppm for Al. LOD's were calculated from 77 background measurements with 95% confidence utilising the Student's t-distribution (see Appendix).

Quartz populations

Based on CL and textural studies (crystal habit, crystal size) five igneous quartz populations can be distinguished in the PGS: phenocryst quartz (I), groundmass quartz (II), and stockscheider quartz (III) in the stock granite and isometric quartz (IV) and comb quartz (V) in the dyke granite.

The stock granite contains rare euhedral quartz phenocrysts (I, 1–5 mm) showing complex growth zoning contrasted with red-brown, violet, and blue CL colours (Fig. 3a). Generally, the phenocrysts have a rounded, red-brown luminescent core. The core is overgrown by blue luminescent oscillatory growth zones. Marginally, the phenocrysts are strongly embayed. The zoning fits the shape of the lobate embayments. Fig. 4a summarises schematically the structural properties of the phenocryst quartz.

The phenocrysts are overgrown by anhedral fine-grained groundmass quartz (II). The groundmass quartz is free of growth zoning and shows weak red-brown CL. Secondary structures are bright halos around radioactive micro-inclusions and non-luminescent, neocrystallised domains. Like the groundmass quartz, the stockscheider quartz (III) is free of growth zoning, shows red-brown luminescence, and contains a number of secondary structures (Fig. 3b).

In the dyke granite and fine-grained layers of the line rock, the quartz forms snowball-textured phenoblasts (IV) 0.2 to 1.5 mm in size (Fig. 3d; Müller and Seltmann 1999). Generally, the snowball quartz has a red- to red-brown CL, whereby bright grey growth zones in the SEM-CL image correspond with zones having a brighter reddish to orange luminescence. The snowball quartz shows continuous growth into the matrix quartz, recognizable by the ramified, dendritic grain boundaries, and penetrates the matrix. The crystals contain common inclusions of the groundmass minerals, such as corroded K-feldspar, mica, metamict zircon, apatite and albite. Fluid and melt inclusions are abundant throughout quartz. Large numbers of albite crystals envelope the phenoblast edge indicating that the quartz pushed the albite tablets away during growth. The phenoblasts show oscillatory growth zoning characterised by planar bordered growth zones with α-quartz habit. The zoning continues into the amoebic crystal margin and into the matrix quartz without changes of the CL properties. Fig. 4b shows the scheme of the structural properties of the snowball quartz. Moreover, the figure illustrates the structural contrasts be-

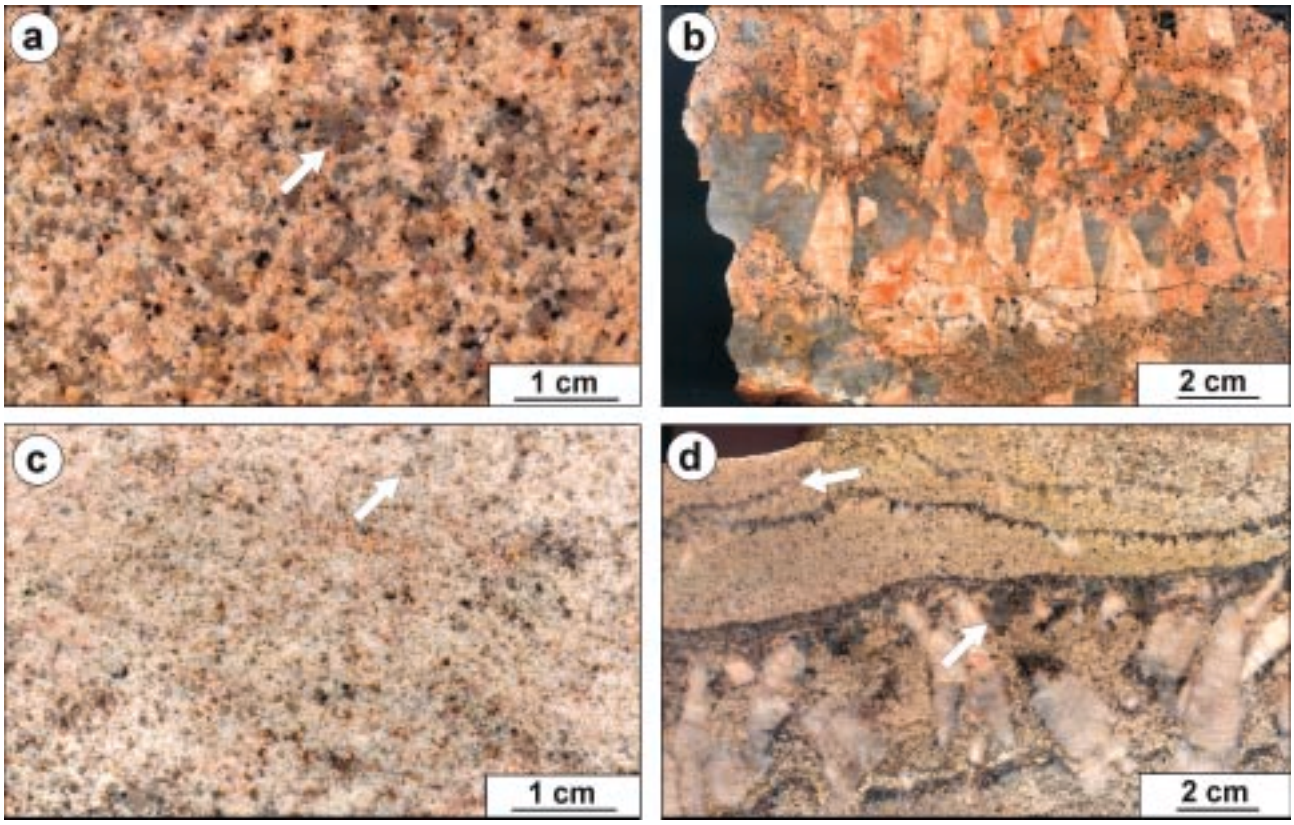

Fig. 2. Hand specimen of textural granite varieties of the PGS. a – Stock granite with rare quartz phenocrysts (arrow); b – Marginal stockscheider at the contact to the Ordovician phyllites. The stockscheider is fragmented by a fine-grained variety of the stock granite; c – Leucocratic dyke granite containing common, small isometric quartz drops (arrow); d – Unidirectional solidification textures (UST) in the upper part of the major dyke granite layer. Locally, oriented comb quartz crystals (arrow) and K-feldspar megacrysts are arranged along fan-like zinnwaldite laminas.

tween quartz phenocrysts (I) and snowball phenoblasts (IV). The comb quartz (V) nucleated at the fan-like zinnwaldite layers of UST exhibits similar growth patterns and CL colours to the snowball quartz (Fig. 3c).

A late- to post-magmatic fluid-driven overprint (e.g. micro fracturing and greisening) causes small-scale dissolution, precipitation and re-equilibration of pre-existing quartz (I–V) along grain boundaries, intra-granular microcracks, and around fluid inclusions resulting in neocrystallised quartz (VI). The neocrystallised quartz has the same crystallographic orientation as the host quartz.

Trace elements in quartz

Locations of the trace element profiles determined by EPMA are shown in Figure 5 and concentrations are compiled in Table 2.

The highest Ti content up to 88 ppm is bounded by blue luminescent growth zones of quartz phenocrysts (I). In contrast, the red-brown luminescent phenocryst core has low Ti, down to 35 ppm. The association of high Ti with blue luminescent quartz is in agreement with previous studies, which proved a relation between high Ti and blue luminescence (Van den Kerkhof et al. 1996, Müller et al. 2000, Müller et al. 2002). Ti distribution in the younger groundmass quartz and stockscheider quartz is more homogeneous than in the phenocryst quartz. The average content is 43 ppm for the groundmass quartz and 41 ppm for the stockscheider quartz, which is similar to the composition of the phenocryst core. Snowball quartz and comb quartz of the dyke granite has low average Ti contents of 26 ppm and 22 ppm, respectively.

In contrast to Ti, the Al content in the phenocryst quartz is relatively constant and low in comparison with those in other quartz populations. Al in the groundmass and

→ Fig. 3. Scanning electron microscope cathodoluminescence images of quartz populations (I–V) in the PGS. a – Zoned phenocryst (I) in the stock granite overgrown by a thin film of groundmass quartz (II) which is free of growth zoning. A number of mica crystals (black) were included during growth of the phenocryst and hindered the growth; b – Stockscheider quartz (III) with common secondary structures, like oriented, healed micro-cracks and small non-luminescent halos which surround fluid inclusions; c – Zoned comb quartz (V) of the unidirectional solidification textures; d – Three examples of zoned, isometric quartz of the dyke granite forming snowball-textured phenoblasts (IV). The CL colours of the snowball quartz are similar to those of the comb quartz.

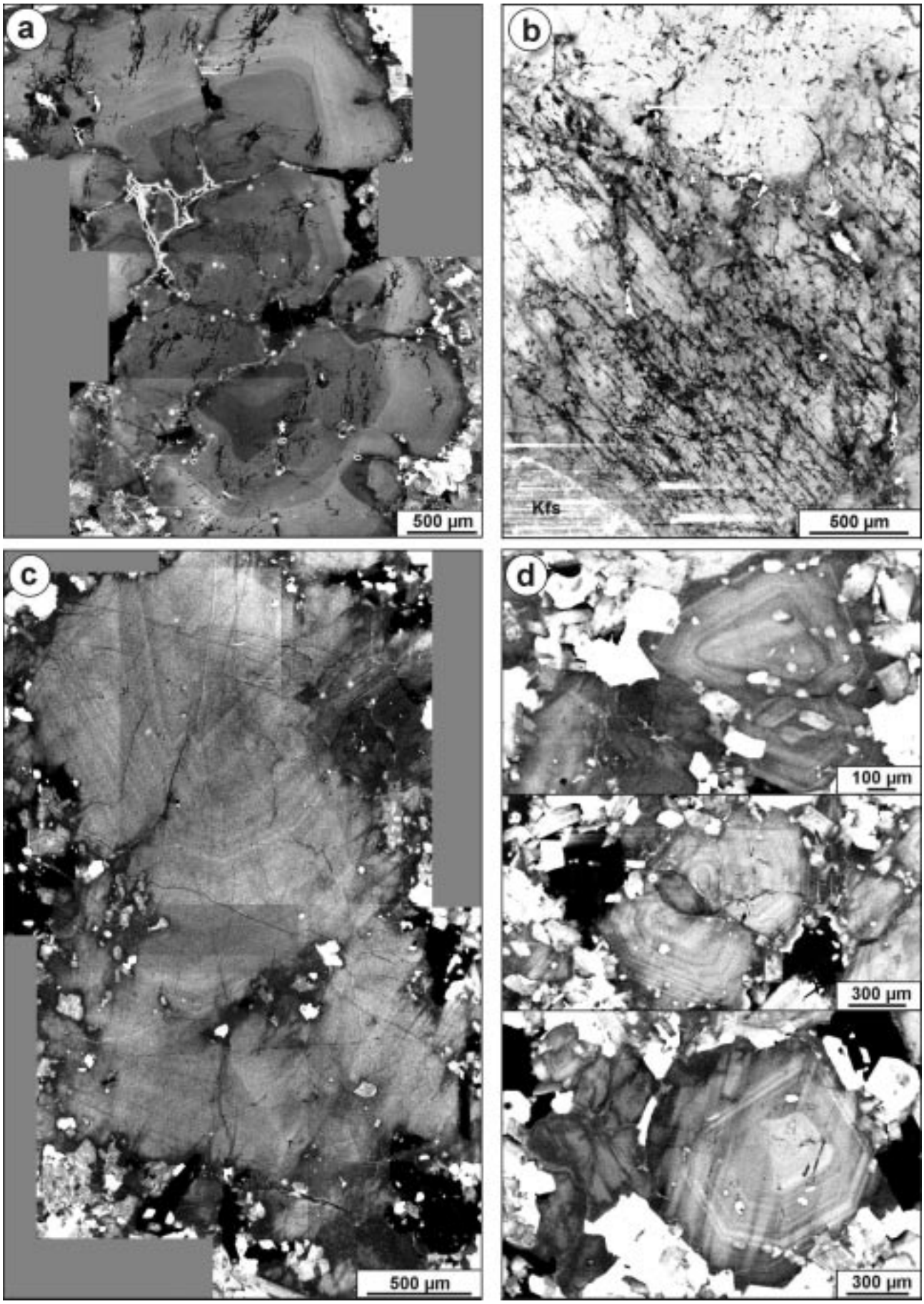
a
500 µm
b
Kfs
500 µm
c
500 µm
d
100 µm
300 µm
300 µm

Table 2. Trace element concentrations (in ppm) of the quartz populations within the PGS. Na were always below the limit of detection, so we do not include it in the table. I – phenocryst quartz, II – groundmass quartz, III – stockscheider quartz, IV – snowball quartz, V – comb quartz, VI – neocrystallised quartz

#	Al	Ti	K	Fe	#	Al	Ti	K	Fe	#	Al	Ti	K	Fe
I-01	279	88	108	51	III-03	476	46	92	28	IV-17	806	26	75	18
I-02	204	59	57	<15	III-04	379	50	68	31	IV-18	1033	29	33	<15
I-03	332	73	135	32	III-05	524	43	187	44	IV-19	453	24	29	15
I-04	220	73	136	30	III-06	434	43	91	44	IV-20	739	39	31	<15
I-05	291	76	126	40	III-07	243	33	27	18	IV-21	354	16	25	17
I-06	265	77	78	31	III-08	482	37	152	51	IV-22	480	32	27	23
I-07	277	81	101	21	III-09	330	47	41	<15					
I-08	322	88	103	50	III-10	360	38	27	17	V-01	610	21	59	16
I-09	283	72	88	26	III-11	383	33	84	34	V-02	372	16	183	16
I-10	318	61	64	21						V-03	338	22	67	<15
I-11	320	73	110	33	IV-01	530	27	38	17	V-04	843	29	193	22
I-12	287	35	84	34	IV-02	306	25	22	<15	V-05	626	15	73	18
I-13	338	49	88	53	IV-03	452	<15	30	<15	V-06	493	23	103	18
I-14	318	44	65	41	IV-04	452	<15	25	<15	V-07	343	16	74	14
I-15	345	41	110	50	IV-05	981	16	53	23	V-08	355	32	58	<15
I-16	445	45	159	90	IV-06	578	30	28	<15	V-09	441	15	92	18
I-17	354	40	109	70	IV-07	582	30	33	16	V-10	307	21	73	24
					IV-08	591	40	52	20	V-11	780	27	149	<15
II-01	459	17	109	18	IV-09	1289	41	37	41					
II-02	393	41	182	58	IV-10	686	<15	37	40	VI-01	62	23	56	74
II-03	416	50	162	29	IV-11	896	34	35	81	VI-02	57	<15	53	51
II-04	356	57	112	44	IV-12	936	31	51	48	VI-03	113	<15	80	126
II-05	309	50	105	35	IV-13	819	27	37	24	VI-04	89	16	83	152
					IV-14	786	28	35	17	VI-05	52	<15	53	76
III-01	386	47	88	26	IV-15	343	25	20	21	VI-06	77	<15	51	37
III-02	384	37	86	19	IV-16	414	17	26	17	VI-07	148	26	78	53

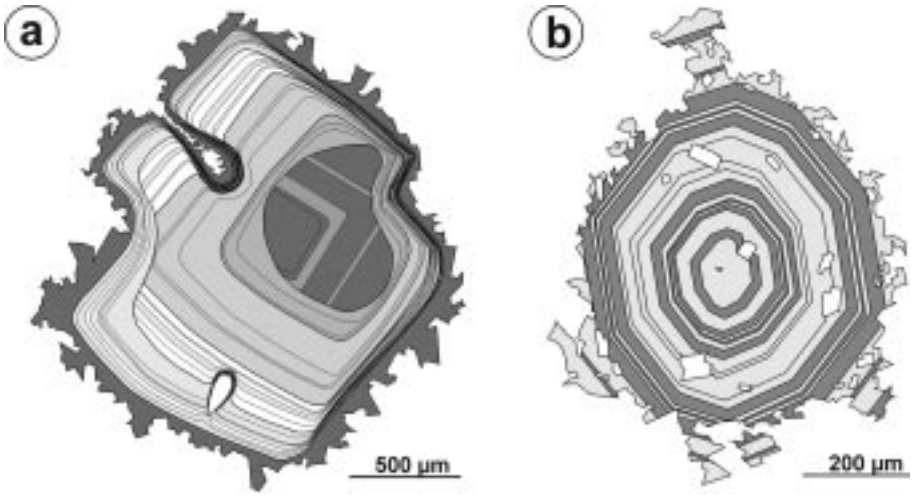

Fig. 4. Schematic growth pattern of quartz phenocrysts (a) and snowball-textured phenoblasts (b).

stockscheider quartz is also homogeneously distributed but it has somewhat higher average concentrations of 387 and 349 ppm, respectively. Snowball quartz as well as comb quartz shows a wide variation of Al from 306 ppm up to 1289 ppm. The contents of Al and Ti show no relation to the zoning in the snowball quartz, in contrast to the phenocryst quartz, where the zoning is related to the Ti concentration. The non-luminescent quartz of healing structures (neocrystallised quartz VI) is depleted in Al and Ti.

The plot of Al and Ti contents of the igneous quartz populations (I–V) yields a trend reflecting the evolution of the magma (Fig. 6a). The early crystallisation stage represented by the quartz phenocrysts is characterised by high Ti and low Al concentrations in the quartz lattice. During further evolution Ti decreases whereas Al increases. The post-magmatic neocrystallised quartz in healed structures does not follow the magmatic trend.

The plot of Al versus K shows two different trends (Fig. 6b). The Al/K ratio in the magmatic quartz of the stock granite (I–III) is about 1 : 0.3, whereby the K concentration is up to 187 ppm. In the snowball quartz (IV) the Al/K ratio amounts 1 : 0.05. The K of the snowball quartz is generally below 50 ppm. The comb quartz shows Al/K ratios between both trends.

Phenocryst quartz and snowball quartz show a positive correlation between the Ti/Fe and the K/Fe concentration ratio (Fig. 6c). The ratios of the neocrystallised quartz also display this correlation and, therefore, it can be concluded that this correlation is not associated with magmatic evolution. The Ti/Fe and the K/Fe ratios of groundmass quartz, stockscheider quartz, and comb quartz plots more scattered due to certain spotty high concentrations of K in these quartz generations.

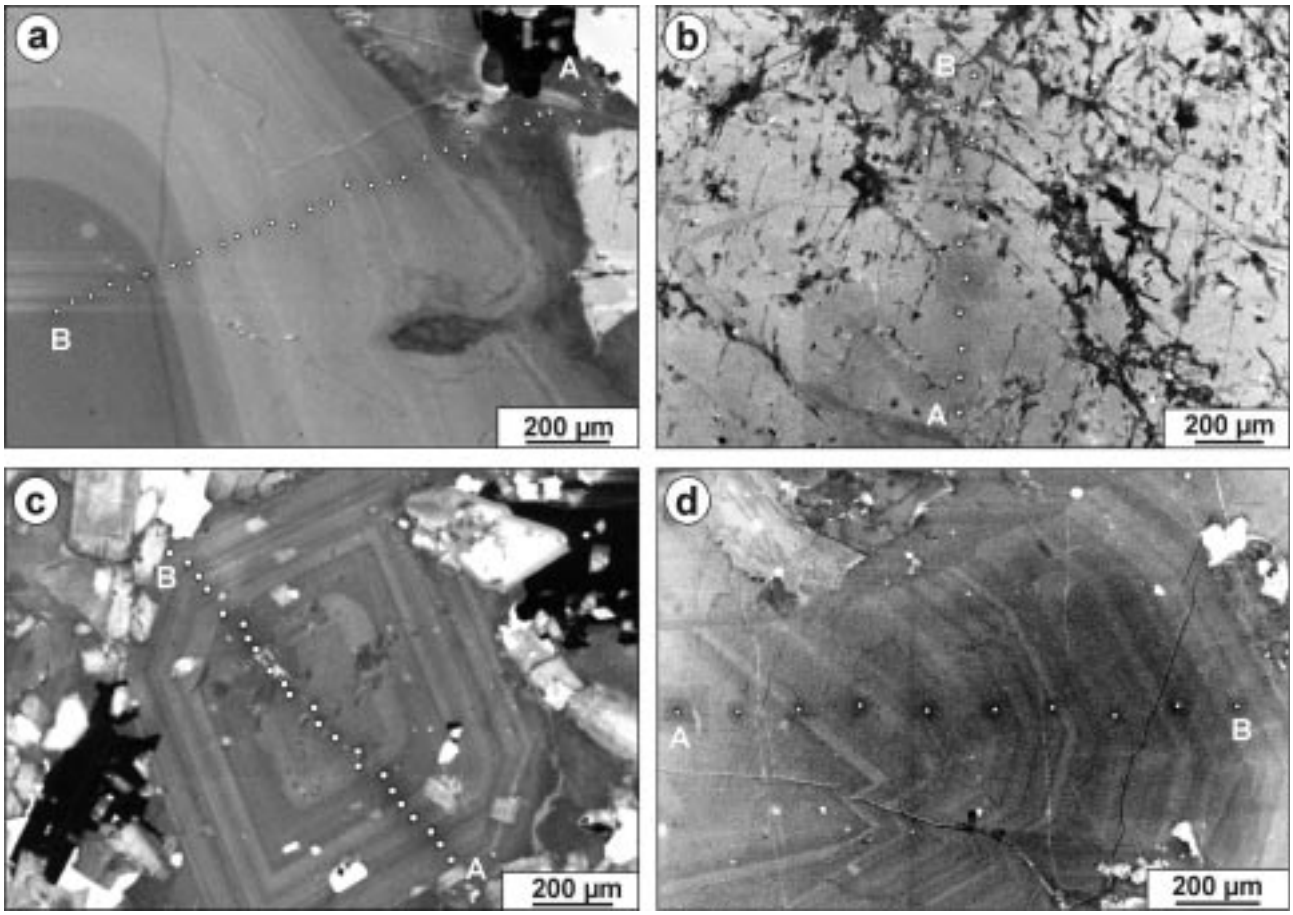

Fig. 5. Location of trace element profiles measured by EPMA. a – Phenocryst quartz overgrown by groundmass quartz. The profile starts in the red-brown luminescent, unzoned groundmass quartz (A), crosses the blue luminescent zones of the phenocryst and ends in the red-brown luminescent phenocryst core (B). The growth zoning of the phenocryst adapts to the shape of lobate embayments, right of the image; b – Stockscheider quartz with common non-luminescent, patchy halos of secondary quartz (black) and healed micro-cracks; c – Snowball quartz; d – Comb quartz.

Discussion

Interpretations of the observed trends of decreasing Ti and increasing Al in quartz during igneous evolution are difficult because the petrogenetic significance of trace elements in quartz is poorly known. First, Stuttner and Leininger (1972) point out that quartz from different magmatic sources has different Ti contents. Recently, Gurbanov et al. (1999) and Larsen et al. (2000) show that the trace element distribution in igneous quartz may follow the petrogenetic history of the quartz-forming melt. Clearly, the trend is related to magmatic evolution, but which parameters control the incorporation of Ti and Al into the quartz lattice?

The significant decrease of Ti and increase of Al in quartz is in contrast to the nearly constant Ti and Al content of the whole rock (see Table 1). Of course, there is a relative increase of Al and decrease of Ti in the more evolved dyke granite in comparison to the stock granite. However, the change of the Ti and Al content in quartz is much more drastic.

The parameters that control Al and Ti incorporation are different for both elements, because they behave in a different way. Al and Ti are the most common trace elements in quartz, which substitute for Si. In contrast to Ti^{4+}, which is independent of the activity of charge compensators, Al^{3+} needs charge compensators, such as Li^+, H^+, K^+, or Na^+ to balance the substitution. These monovalent ions enter interstitial positions in channels running parallel to the c-axis (e.g. Bambauer 1961, Dennen et al. 1970, Lehmann and Bambauer 1973, Weil 1984). The berlinite substitution ($2Si^{4+} = Al^{3+} + P^{5+}$) known in feldspars (Simpson 1977) has not been found in natural quartz.

High Ti concentrations are typical for quartz formed at temperatures >500 °C and at high pressure, such as in granulites (Blankenburg et al. 1994, Van den Kerkhof and Müller 1999). Thomas (1992) calculated the maximum crystallisation depth of quartz phenocrysts in tin granites of the Krušné hory/Erzgebirge of about 21 km, based on microthermometric studies of silicate melt inclusions. Therefore, high crystallisation temperature and pressure during the early stage of the magma crystallisation are responsible for the high average Ti in the quartz phenocrysts. The variation of Ti between single growth zones may result

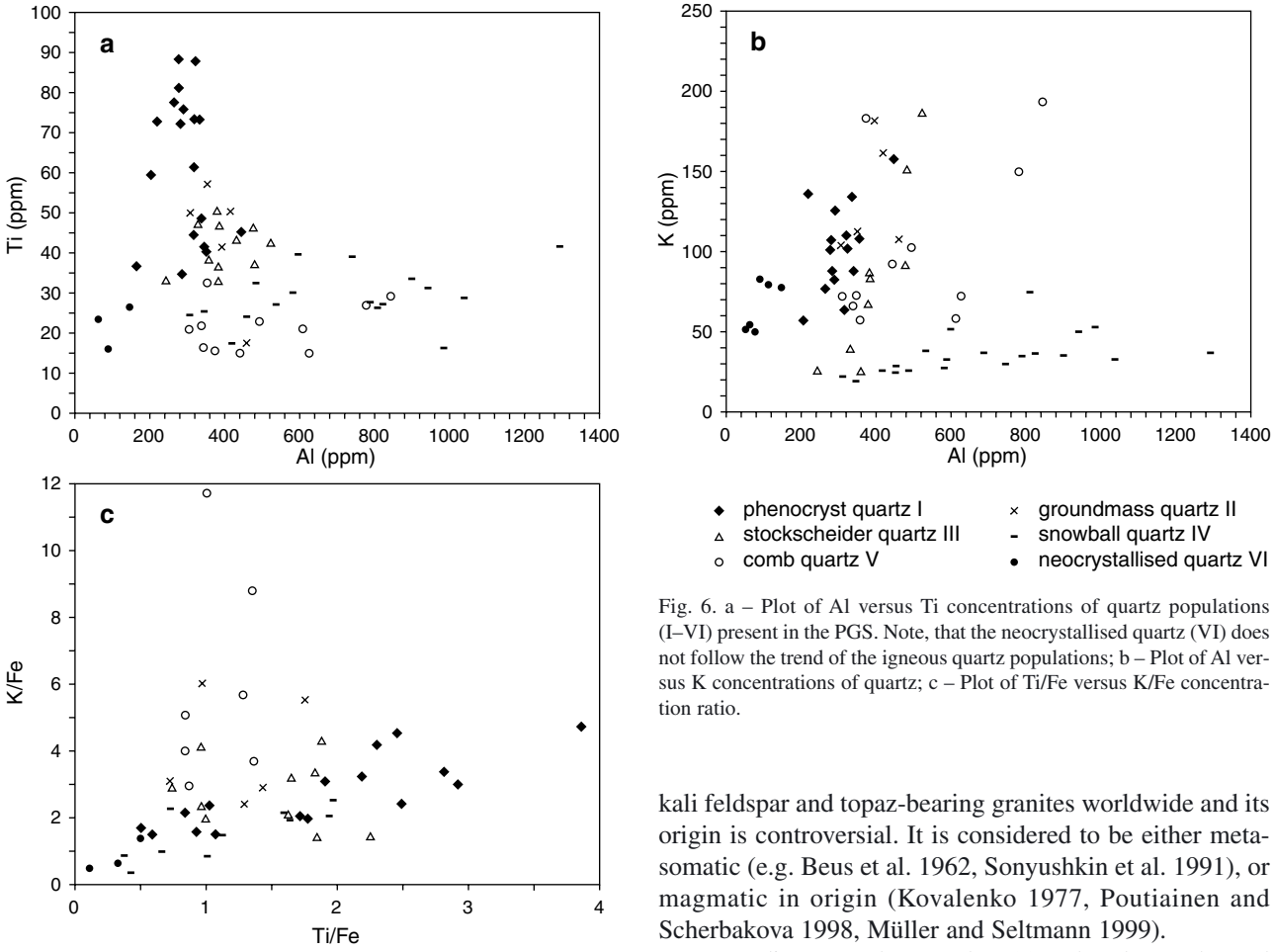

Fig. 6. a – Plot of Al versus Ti concentrations of quartz populations (I–VI) present in the PGS. Note, that the neocrystallised quartz (VI) does not follow the trend of the igneous quartz populations; b – Plot of Al versus K concentrations of quartz; c – Plot of Ti/Fe versus K/Fe concentration ratio.

from crystal fluctuation and ascent, whereby the crystal is exposed to different temperatures, pressures, as well as to variation of the Ti content in the melt.

Both the groundmass quartz (II) and the stockscheider quartz (III) have similar, moderate Ti and Al concentrations indicating that both populations crystallised contemporaneously from the same magma.

In the following we discuss the causes of the high Al in the snowball quartz (IV) and comb quartz (V) which occur in the dyke granite. Both quartz populations have similar trace element signature. Furthermore, similar CL properties and growth patterns support the assumption that both populations crystallised from the same fluid-enriched magma pulse. This is in contrast to earlier studies by Breiter et al. (1997) who assumes that the comb quartz of the pegmatite like bands of the line rock crystallised later than the dyke granite host rock and form a different fluid-enriched melt. The crystal size and crystal habit contrast between snowball quartz and comb quartz may be explained by different nucleation processes. In contrast to Lowenstern and Sinclair's (1996) model for comb quartz formation, both the comb quartz and the snowball quartz grew from melt. The melt is preserved as melt inclusions in both quartz populations (see also Breiter et al. 1997).

The snowball texture is typical for highly evolved alkali feldspar and topaz-bearing granites worldwide and its origin is controversial. It is considered to be either metasomatic (e.g. Beus et al. 1962, Sonyushkin et al. 1991), or magmatic in origin (Kovalenko 1977, Poutiainen and Scherbakova 1998, Müller and Seltmann 1999).

According to Holten et al. (1997) the observed zonal texture of the snowball quartz and comb quartz mostly reflects external fluctuations in an open system (e.g., degassing) and is not a product of self-organisation. Zinnwaldite layers partially envelope the edge of comb quartz and of K-feldspar megacrysts indicating that these large crystals put off the zinnwaldite layers during growth in a viscous environment (see Fig. 2d). The trigonal habit of the zoning, the frequently enclosed groundmass albites and the occurrence of melt inclusions indicate a growth of the snowball quartz of the PGS in a nearly non-convecting and fluid-saturated crystal mush at a temperature of <600 °C (at <1 kbar). To reach such low temperatures, particularly at the shallow depth at which the PGS is emplaced fluxing agents like Li, B, F and water must be added to the magma. High F (2.2 wt%), high P_2O_5 (2.6 wt%), and about 7.5±0.8 eq.-wt% water determined from melt inclusions in the dyke granite (Breiter et al. 1997) should have dramatically suppressed the solidus temperature (e.g. Manning 1981). The extrapolated solidus temperature (Thomas et al.1996) is 610 ± 26 °C for the melt of the dyke granite, which is in agreement with our observations.

The occurrence of ghost K-feldspar phenocrysts and mica in the dyke granite with a similar element signature and CL characteristics to the K-feldspar and mica in the stock granite (Breiter 2001) provides evidence that quartz phenocrysts were also originally present in the dyke granite, but

they were completely cannibalised. P-enriched rims of K-feldspar and Li-enriched rims of mica found only in the dyke granite document a distinctly more evolved environment enriched in phosphorus and fluorine. Other features that significantly support subsolidus processes are (1) the disappearance of "common" accessory minerals in the dyke granites (Förster 2001) and (2) the resetting of the oxygen isotope thermometers to lower submagmatic temperatures (Žák et al. 2001). The latter is a result of the activity of high-$\delta^{18}O$ fluids, whereas low-$\delta^{18}O$ fluids are not involved in this process.

The increase of Al in the snowball quartz and comb quartz may by related to the evolution of magma composition, e.g., to the increasing content of lithophile elements, particularly Li^+, K^+, and Na^+, which are the main charge compensating ions of substitutional Al^{3+}. Beside these elements, hydroxyl groups and adsorbed H_2O act as charge compensators for $[2AlO_4/M^+]^-$ defects, where M^+ is a combination of Li, K, and Na ions (Bambauer et al. 1963, Maschmeyer and Lehmann 1983, Kronenberg et al. 1986, Stenina 1995). Therefore, the uptake of Al into the quartz lattice may be partially controlled by the presence of Li^+, K^+, and Na^+ and water in the melt. Substitutional P^{5+} may also function as a charge compensator of substitutional Al^{3+} as is known from feldspar (Simpson 1977). Therefore, the high P^{5+} content of up to 2 wt% P_2O_5 (Breiter 2001) in the line rock may also influence the Al^{3+} content in the quartz lattice. The high Al in the snowball quartz and in the comb quartz may, therefore, reflect the enrichment of lithophile elements and water in the magma of the dyke granite.

However, spotty high Al in the snowball quartz and comb quartz (>500 ppm) suggest that Al is not only structurally incorporated, but that it also occurs as impurity clusters or inclusions (Flicstein and Schieber 1974, Blankenburg et al. 1994, Brouard et al. 1995, Götze et al. 1999, Mullis and Ramseyer 1999, Müller et al. 2002). Caused by the larger ion radius of Al^{3+} (r = 0.47 Å) in comparison to Si^{4+} (r = 0.34 Å) such high amounts of structurally incorporated Al^{3+} should cause an extreme deformation and weakening of the quartz lattice. Structurally incorporated Al in igneous quartz typically ranges up to 400 ppm (Watt et al. 1997, Morgan et al. 1998, Müller et al. 2000). Surprisingly, analyses of the snowball quartz with very high Al have low K (Fig. 6b) although K functions as charge compensator for Al. However, the spotty high Al suggests that Al is accumulated within submicrometer sized inclusions.

In general, high impurity densities in quartz correlate with fast growth rates in synthetic crystals (Brice 1985). Such growth rates (up to >3 mm/day) are 50 times faster than the highest known growth rates for skeletal magmatic high-quartz (Swanson and Fenn 1986). Temperature and pressure alone do not appear to have a significant affect on Al substitution in quartz (Scotford 1975, Pavlishin et al. 1978, Stavrov et al. 1979). The Al uptake may be more sensitive to variations in growth rate. The characteristic zoning pattern, the frequently enclosed groundmass minerals and the dendritic crystal margins point to rapid crystal growth during multiple degassing pulses.

Another source of Al in the snowball quartz and comb quartz may be impurity clusters that originate from replaced and dissolved albite crystals during the blastic growth of quartz.

Low trace element concentrations in neocrystallised quartz point to a systematic recovery of defect centres and to trace element redistribution in the quartz lattice, whereby impurities are probably released from quartz during solid-state neocrystallisation (Müller et al. 2002). Also the very low CL intensity indicates a low defect concentration in this neocrystallised quartz.

Conclusion

The examination of quartz populations in the PGS gives evidence for three main stages of crystallisation: (1) quartz phenocrysts representing the early stage of magma evolution, (2) stockscheider quartz and groundmass quartz of the stock granite reflecting the solidification conditions of the stock granite, and (3) the snowball quartz and comb quartz of the dyke granite that crystallised from a highly evolved, residual melt.

We observe a general trend of the trace element distribution in the igneous quartz populations (I–V) reflecting the evolution of the magma: a decrease of Ti and an increase of Al.

The increase of the lithophile elements (Li, Na, Al, P, K) and of the water content in the magma and the decrease of Ti, crystallisation temperature and pressure are assumed to be predominantly responsible for the trend. Extremely high Al in quartz may also result from high crystal growth rate. The Ti-enriched phenocrysts (I) originated in greater depth represent the early less evolved magmatic stage. Groundmass quartz (II) and stockscheider quartz (III) are the result of crystallisation from the stock granite in the intrusion level.

The Al-rich snowball quartz (IV) and comb quartz (V) of the UST crystallised at low temperatures (<600 °C) and pressures (<1 kbar) from a highly evolved, fluid-enriched magma. A spotty high Al concentration in both quartz populations is mainly interpreted as submicrometer sized inclusions incorporated during fast crystal growth. The zoning pattern of the snowball quartz and comb quartz is explained by periodic degassing during melt cooling in the granite roof. Highly reactive fluids exsolved in the late magmatic stage from the melt cause the resorption and, partially, the complete solution of quartz and feldspar phenocrysts of the early crystallisation stage. Summarising, the dyke granite in general is not a product of metasomatic overprinting of the stock granite, but the product of crystallisation of a different, more fractionated melt.

Acknowledgements. We thank A. M. van den Kerkhof, H.-J. Behr, and R. Seltmann for discussion and critical comments. We are also indebted to R. B. Larsen and W. Siebel for reviews and fruitful discussions. This work was funded by the Deutsche Forschungsgemeinschaft (MU 1717/2-1) and by the German Bundesministerium für Bildung und Forschung (CZE 00/011).

References

Armstrong J. T. (1991): Quantitative elemental analysis of individual microparticles with electron beam instruments. In: Heinrich K. F. J., Newbury D. E. (eds) Electron probe quantification. Plenum Press, pp. 261–315.

Balashov V. N., Zaraisky G. P., Seltmann R. (2000): Fluid-magma interaction and oscillatory phenomena during crystallisation of granitic melt by accumulation and escape of water and fluorine. Petrology 8, 563–585.

Bambauer H. U. (1961): Spurenelementgehalt und –Farbzentren in Quarzen aus Zerrklüften der Schweizer Alpen. Schweiz. Mineral. Petrogr. Mitt. 41, 335–369.

Bambauer H. U., Brunner G. O., Laves F. (1963): Merkmale des OH-Spektrums alpiner Quarze (3µ-Gebiet). Schweiz. Mineral. Petrogr. Mitt. 43, 259–268.

Beus A. A., Severov E. A., Sitnin A. A., Subbotin K. D. (1962): Albitized and greisenized granites (apogranites). Nauka, Moscow (in Russian).

Blankenburg H-J, Götze J, Schulz J. (1994): Quarzrohstoffe. Deutscher Verlag für Grundstoffindustrie, Leipzig-Stuttgart.

Breiter K. (2001): Phosphorus- and fluorine-rich granite system at Podlesí. In: Breiter K. (ed) Phosphorus- and Fluorine-rich Granites. Abstracts – Excursion guide – Program. Int. Workshop Podlesí, Czech Geol. Surv., Praha, 54–78.

Breiter K. (2002): From explosive breccia to unidirectional solidification textures: Magmatic evolution of a phosphorus- and fluorine-rich granite system (Podlesí, Krušné hory Mts., Czech Republic). Bull. Czech Geol. Surv., 77, 2, 67–92.

Breiter K., Frýda J., Seltmann R., Thomas R. (1997): Mineralogical evidence for two magmatic stages in the evolution of an extremely fractionated P-rich rare-metal granite: the Podlesí Stock, Krušné hory, Czech Republic. J. Petrol. 38, 1723–1739.

Brice J. C. (1985): Crystals for quartz resonators. Rev. Mod. Phys. 57, 105–146.

Brouard S., Breton J., Girardet G. (1995): Small alkali metal clusters on (001) quartz surface: adsorption and diffusion. J. Molecular Struct. (Theochem) 334, 145–153.

Chlupáčová M., Breiter K. (1998): Physical properties of extremely fractionated P-rich rare-metal granite: borehole PTP-1, the Podlesí stock, Krušné hory Mts., Czech Republic. Acta Univ. Carol., Geol. 42, 28–31.

Dennen W. H., Blackburn W. H., Quesada A. (1970): Aluminium in quartz as a geothermometer. Contr. Mineral. Petrol. 27, 332–342.

D'Lemos R. S., Kearsley A. T., Pembroke J. W., Watt G. R., Wright P. (1997): Complex quartz growth histories in granite revealed by scanning cathodoluminescence techniques. Geol. Mag. 134, 549–552.

Flicstein J., Schieber M. (1974): Microsegregation of impurities in hydrothermally-grown quartz crystals. J. Cryst. Growth 24/25, 603–609.

Förster H.-J. (2001): The radioactive accessory-mineral assemblage of the Podlesí granite-pegmatite system, western Krušné hory: Implications to intrusion age and magmatic/hydrothermal fluid-rock interaction. In: Breiter K. (ed) Phosphorus- and Fluorine-rich Granites. Abstracts – Excursion guide – Program. Int. Workshop Podlesí, Czech Geol. Surv., Praha, 14–15.

Götze J., Plötze M., Fuchs H., Habermann D. (1999): Defect structure and luminescence behaviour of agate – results of electron paramagnetic resonance (EPR) and cathodoluminescence (CL) studies. Min. Mag. 63, 149–163.

Gurbanov A. G., Chernukha F. P., Koshchug D. G., Kurasova S. P., Fedyushchenko S. V. (1999): EPR spectroscopy and geochemistry of rock-forming quartz as an indicator of the superimposed processes in rocks of igneous associations of various ages in the Greater Caucasus. Geochem. Int. 37, 519–532.

Holten T., Jamtveit B., Meakin P., Cortini M., Blundy J., Austrheim H. (1997): Statistical characteristics and origin of oscillatory zoning in crystals. Amer. Mineralogist 82, 596–606.

Kirkham R. V., Sinclair W. D. (1988): Comb quartz layers in felsic intrusions and their relationship to porphyry deposits. In: Taylor R. P., Strong D. F. (eds) Recent advances in the geology of granite-related mineral deposits. CIM Spec. Vol. 31, 50–71.

Kovalenko V. I. (1977): Petrology and geochemistry of rare-metal granitoids. Nauka, Novosibirsk (in Russian).

Kronenberg A. K., Kirby S. H., Aines R. D., Rossmann G. R. (1986): Solubility and diffusional uptake of hydrogen in quartz at high water pressures: implications for hydrolytic weakening in the laboratory and within the earth. Tectonophysics 172, 255–271.

Larsen R. B., Polvé M., Juve G. (2000): Granite pegmatite quartz from Evje-Iveland: trace element chemistry and implications for the formation of high-purity quartz. Bull. Geol. Surv. Norway 436, 57–64.

Lehmann G., Bambauer H. V. (1973): Quarzkristalle und ihre Farben. Angew. Chem. 7, 281–289.

Lhotský P., Breiter K., Bláha V., Hrochová H. (1988): Economic-geological investigations of Sn-mineralisation near Podlesí in the western Krušné hory. Internal Report, Czech Geol. Surv., Praha (in Czech).

Lowenstern J. B., Sinclair W. D. (1996): Exsolved magmatic fluid and its role in the formation of comb-layered quartz at the Cretaceous Logtung W-Mo deposit, Yukon Territory, Canada. Trans. Royal Soc. Edinburgh 87, 291–303.

Manning D. A. C. (1981): The effect of fluorine on liquidus phase relationships in the system Qz-Ab-Or with excess Water at 1kb. Contrib. Mineral. Petrol. 76, 206–215.

Maschmeyer D., Lehmann G. (1983): A trapped-hole centre causing rose coloration of natural quartz. Z. Kristallogr. 163, 181–196.

Morgan G. B., London D., Luedke R. G. (1998): Petrochemistry of late Miocene peraluminous silicic volcanic rocks from the Morococala field, Bolivia. J. Petrology 39, 601–632.

Müller A., Lennox P., Trzebski R. (2002): Cathodoluminescence and micro-structural evidence for crystallisation and deformation processes of granites in the Eastern Lachlan Fold Belt (SE Australia). Contr. Mineral. Petrology, (in press).

Müller A., Seltmann R. (1999): The genetic significance of snowball quartz in high fractionated tin granites of the Krušné hory/Erzgebirge. In: Stanley C. J. et al. (eds) Mineral deposits: processes to processing. Volume 1. Balkema, Rotterdam, pp. 409–412.

Müller A., Seltmann R., Behr H.-J. (2000): Application of cathodoluminescence to magmatic quartz in a tin granite – case study from the Schellerhau Granite Complex, Eastern Erzgebirge, Germany. Mineralium Deposita 35, 169–189.

Mullis J., Ramseyer K. (1999): Growth related Al-uptake in fissure quartz, Central Alps, Switzerland. Terra Nostra 99, 6, 209.

Pavlishin V. I., Mazykin V. V., Matyash I. V., Voznyak D. K. (1978): Variations in the proportion of substitutional aluminium during growth of a quartz crystal. Geochem. Int. 15, 158–165.

Poutiainen M., Scherbakova T. F. (1998): Fluid and melt inclusion evidence for the origin of idiomorphic quartz crystals in topaz-bearing granite from the Salmi batholith, Karelia, Russia. Lithos 44, 141–151.

Reyf F. G., Seltmann R., Zaraisky G. P. (2000): The role of magmatic processes in the formation of banded Li, F-enriched granites from the Orlovka tantalum deposit, Transbaikalia, Russia: microthermometric evidence. Canad. Mineralogist 38, 915–936.

Schneider N. (1993): Das lumineszenzaktive Strukturinventar von Quarzphänokristen in Rhyolithen. Göttinger Arb. Geol. Paläont. 60, 1–81.

Scotford D. M. (1975): A test of aluminium in quartz as a geothermometer. Amer. Mineralogist 60, 139–142.

Shannon J. R., Walker B. M., Carten R. B., Geraghty E. P. (1982): Unidirectional solidification textures and their significance in determining relative ages of intrusions at the Henderson Mine, Colorado. Geology 10, 293–297.

Simpson D. R. (1977): Aluminium phosphate variants in feldspars. Amer. Mineralogist 62, 351–355.

Sonyushkin V. E., Sukhorukov Y. T., Scherbakova T. F. (1991): P-T environment of crystallization of quartz in granites of the Salmi batholith, Russian Karelia. In: Haapala I., Rämö O.T. (eds) Sympo-

sium on Rapakivi Granites and Related Rocks. Geol. Surv. Finland Guide 34, p.47.

Stavrov O. D., Moiseyev B. M., Rakov L. T. (1979): Relation between content of alkali metals and concentration of aluminium centers in quartz. Geochem. Int. 15, 5–10.

Stenina N. G. (1995): Energy aspect in the formation of granitic magma and ore deposits. In: Pašava J., Křibek B., Žák K. (eds) Mineral deposits: from their origin to their environmental impacts. Balkema, Rotterdam, 539–542.

Stuttner L. J., Leininger R. K. (1972): Comparison of the trace element content of plutonic, volcanic and metamorphic quartz from southwestern Montana. Bull. Geol. Soc. Amer. 83, 1855–1862.

Swanson S. E., Fenn P. M. (1986): Quartz crystallisation in igneous rocks. Amer. Mineralogist 71, 331–342.

Táborská Š., Breiter K. (1998): Magnetic anisotropy of an extremely fractionated granite: the Podlesí Stock, Krušné hory Mts., Czech Republic. Acta Univ. Carol. Geol. 42, 147–149.

Thomas R. (1992): Results of investigations on melt inclusions in various magmatic rocks from the northern border of the Bohemian Massif. In: Kukal Z. (ed) Proceed. 1st Int. Conf. Bohemian Massif. Czech Geol. Surv., Prague, 298–306.

Thomas R., Rhede D., Trumbull R. B. (1992): Microthermometry of volatile-rich silicate melt inclusions in granitic rocks. Z. Geol. Wiss. 24, 505–526.

Van den Kerkhof A. M., Kronz A., Simon K. (2001): Trace element redistribution in metamorphic quartz and fluid inclusion modification: observations by cathodoluminescence. XVI ECROFI, Porto 2001, Fac. Ciências Porto, Dep. Geol., Memória 7, 447–450.

Van den Kerkhof A. M., Müller A. (1999): Fluid inclusion re-equilibration and trace element redistribution in quartz: observations by cathodoluminescence. ECROFI XV abstracts and program, Terra Nostra 99, 6, 161–162.

Van den Kerkhof A. M., Scherer T., Riganti A. (1996): Cathodoluminescence and EPR analysis of Archean quarzites from the Nondweni Greenstone Belt, South Africa. Abstracts SLMS International Conference on Cathodoluminescence, Nancy, Sept. 1996, p. 75.

Watt G. R., Wright P., Galloway S., McLean C. (1997): Cathodoluminescence and trace element zoning in quartz phenocrysts and xenocrysts. Geochim. Cosmochim. Acta 61, 4337–4348.

Weil J. A. (1984): A review of electron spin spectroscopy and its application to the study of paramagnetic defects in crystalline quartz. Phys. Chem. Minerals 10, 149–165.

Weiss Z., Rieder M., Smrčok L., Petříček V., Bailey S. W. (1993): Refinement of the crystal structures of two “protolithionites”. Eur. J. Mineral. 5, 493–502.

Žák K., Pudilová M., Breiter K. (2001): Oxygen isotope study of the highly fractionated Podlesí granite system – preliminary data. In: Breiter K. (ed) Phosphorus- and Fluorine-rich Granites. Abstracts – Excursion guide – Program. Int. Workshop Podlesí, Czech Geol. Surv., Praha, 34–35.

Appendix

Limits of detection (LOD) were calculated from 77 background measurements with 95% confidence utilising the Student's t-distribution according to the following equation (Table 3):

$$I_{LOD} = t_z\,(P;f)\,\sigma_{BG}$$

where I_{LOD} = intensity of the LOD [cts]; σ_{BG} = standard deviation of the average background; t_z (P;f) = the Student's t for binomial limitation determined by the confidence P and the degrees of freedom f = n – 2, where n is the number of background measurements. The Student's t with 95% confidence amounts 1.99 for 77 background measurements.

For comparison also the common method for calculating LOD, given by:

$$I_{LOD} = 3\ \sqrt{BG}$$

for an single measurement was estimated.

BG are the total accumulated counts of the background signal. (“LOD by single measurement”). Both methods give comparable results, but we prefer the random sampling using Student's t-test. The latter is more sensitive due to systematic errors and the occurrence of drift-phenomena.

The concentration of LOD C_{LOD} is calculated using the factor of the linear calibration of total intensity vs. concentration of an element (see Table 3):

$$C_{LOD}\ [\text{ppm}] = \text{factor} * I_{LOD}$$

(Due to the constant composition of the matrix SiO_2, there would be no change in the ZAF-factors, hence a linear calculation is reliable.)

Table 3. Limits of detection (LOD). The average background (BG) is the mean of the total acquired counts for each element using 150 seconds counting time on each side of the peak (20 kV and 80 nA).

element	counting time peak	each BG	average BG	factor	LOD by n=77 measurements		LOD by single measurement	
	[s]	[s]	[cts]	(lin. calib.)	$I_{LOD} = 1.99 * \sigma_{BG}$ [cts]	C_{LOD} [ppm]	$I_{LOD} = 3 * \sqrt{}_{BG}$ [cts]	C_{LOD} [ppm]
Al	300	150	42580	0.016	615	10	619	10
K	300	150	14800	0.030	365	11	365	11
Ti	300	150	33060	0.028	540	15	545	15
Fe	300	150	36040	0.029	520	15	570	17